Hypothalamic control of male aggression-seeking behavior

Annegret L Falkner[1], Logan Grosenick[2], Thomas J Davidson[3], Karl Deisseroth[2,4] & Dayu Lin[1,5,6]

In many vertebrate species, certain individuals will seek out opportunities for aggression, even in the absence of threat-provoking cues. Although several brain areas have been implicated in the generation of attack in response to social threat, little is known about the neural mechanisms that promote self-initiated or 'voluntary' aggression-seeking when no threat is present. To explore this directly, we utilized an aggression-seeking task in which male mice self-initiated aggression trials to gain brief and repeated access to a weaker male that they could attack. In males that exhibited rapid task learning, we found that the ventrolateral part of the ventromedial hypothalamus (VMHvl), an area with a known role in attack, was essential for aggression-seeking. Using both single-unit electrophysiology and population optical recording, we found that VMHvl neurons became active during aggression-seeking and that their activity tracked changes in task learning and extinction. Inactivation of the VMHvl reduced aggression-seeking behavior, whereas optogenetic stimulation of the VMHvl accelerated moment-to-moment aggression-seeking and intensified future attack. These data demonstrate that the VMHvl can mediate both acute attack and flexible seeking actions that precede attack.

Individuals may seek out opportunities to attack, even in the absence of overt threat[1–9]. In the wild, male mice exhibit stalking behavior if they suspect foreign encroachment[10], and wild chimpanzees will engage in coalitionary aggressive actions on neighboring social groups for reasons seemingly unrelated to defense[11]. Aggression-seeking in humans can take diverse physical forms, ranging from playground bullying to military provocation, and models of human violence routinely posit a division between 'reactive' aggression, which occurs in response to direct confrontation, and 'proactive' aggression, which does not depend on immediate cues[12,13]. Under laboratory conditions, acts of aggression have been shown to be rewarding, such that animals will show operant learning[1–9] for future aggression and will exhibit conditioned place preference for a location associated with a previously successful aggressive encounter[14]. However, despite the prevalence of aggression-seeking behaviors across vertebrate species, its underlying neural mechanisms are poorly understood.

The medial hypothalamus is a key component of the vertebrate social decision-making network[15] and has a long-established role in inter-male aggression[16–19]. A subnucleus of this area, the VMHvl, was recently identified as a critical locus for generating attack in male mice: silencing this area suppresses naturally occurring inter-male attack, whereas optogenetic stimulation promotes approach and attack of suboptimal targets, including females and inanimate objects[20–22]. However, it has been difficult to discern whether these manipulations change the expression of aggressive action or induce behavioral change by modulating levels of aggression-seeking behavior. More directly, does VMHvl stimulation evoke attack itself or change the motivation for future attack? Recent electrophysiological recordings in freely interacting mice demonstrated that VMHvl neurons are activated not only during attack and investigation of a male conspecific, but also by proximity to a pure olfactory cue (male urine)[23], making it

difficult to discern whether activity changes before attack represent changing sensory or motivational variables. This difficulty in isolating motivational signals during free social interactions necessitates a shift toward the use of social tests with greater behavioral control, where signals that predict future aggression can be temporally separated from the aggression itself.

We adopted and optimized a self-initiated aggression (SIA) task[1,6,9] that isolates the seeking phase of aggression from attack in a series of aggression-seeking trials. Using a combination of techniques for electrophysiology, optical recording and functional manipulation, we found a previously unknown role for the VMHvl in flexibly signaling and mediating aggression-seeking behavior.

RESULTS

### Aggressive males show aggression-seeking behavior

We trained male mice on the SIA task to identify individuals with a predilection for aggression seeking. We first tested animals' 'baseline' level of aggression by using a resident-intruder test, a classic test for reactive inter-male aggression ($N = 76$ mice trained on the SIA task, 69 of 76 mice baseline tested; **Fig. 1a**)[24,25]. Following this resident-intruder pre-test, we trained each mouse for 6–10 d using the SIA procedure (**Fig. 1b**). During each day of the 35-min training session, a panel with two nosepoke ports was introduced to the home cage. If mice poked the designated 'social' port during training, they received free access to a submissive, highly defeated male for a short interaction (a 5–10-s behavioral bout) following a brief wait period of 5.5 ± 1.4 s (mean $\pm$ s.d.). Poking the second 'null' port triggered no interaction event. The relative preference for the social port over the null port across successive days of training was used to quantify task learning. Animals had full control over the trial rate and no additional reinforcements such as food or water were given at any time during training or testing.

[1]Institute of Neuroscience, New York University School of Medicine, New York, New York, USA. [2]Department of Bioengineering, Neuroscience Program, Stanford University, Stanford, California, USA. [3]Department of Bioengineering and CNC Program, Stanford University, Stanford, California, USA. [4]Howard Hughes Medical Institute, Stanford University, Stanford, California, USA. [5]Department of Psychiatry, New York University School of Medicine, New York, New York, USA. [6]Center for Neural Science, New York University, New York, New York, USA. Correspondence should be addressed to A.L.F. (annegret.falkner@nyumc.org) or D.L. (dayu.lin@nyumc.org).

Figure 1 Male mice will seek opportunities to attack in the absence of threat-provoking cues. (**a**,**b**) Mice were screened for aggression using the resident-intruder procedure (**a**) and then trained on the self-initiated aggression task (**b**), which separates the aggression-seeking phase from the social interaction. (**c**,**d**) Average learning curves for all learners (**c**, $N = 43$ of 76 mice) showed increased response rates for the social port (blue) across training, whereas non-learners (**d**, $N = 33$ of 76 mice) showed no increase relative to the null port (red). Insets, behavior of example learner and non-learner individuals. (**e**) Percent trials to social port (trials to social port/total trials × 100) increased for learners (black) relative to non-learners (gray) across training. (**f**) Learner males exhibited more aggression during the resident intruder test than non-learner males ($t(67) = 2.201$, $P = 0.031$, unpaired t test). (**g**) Comparison of aggression level exhibited during resident intruder test to speed of task learning ($N = 39$ learners). (**h**) Behavioral reversal when contingency was reversed. Blue and red show testing days where right-hand and left-hand ports, respectively, were associated with the submissive male reinforcement (comparison of final days of reversal, $t(6) = 13.3315$, $P = 1.102 \times 10^{-5}$; $t(6) = -4.447$, $P = 0.004$, paired t test; single-day comparisons for day 1: $t(6) = 5.900$, $P = 0.001$; day 2: $t(6) = 5.077$, $P = 0.002$; day 6: $t(6) = -3.392$, $P = 0.015$; day 9: $t(6) = 2.818$, $P = 0.030$; t test, $N = 7$ mice). (**i**) Behavior of a representative animal (one of eight) during the non-submissive replacement test. Each tick represents one nosepoke. (**j**) Response rate across animals was reduced for a non-submissive male ($t(7) = 3.548$, $P = 0.009$, paired t test, $N = 8$ mice), and response rate recovered when access to a submissive male was resumed ($t(7) = -4.167$, $P = 0.004$, paired t test, $N = 8$). In **c**–**h** and **j**, data are presented as mean ± s.e.m. *$P < 0.05$, **$P < 0.01$, ***$P < 0.001$.
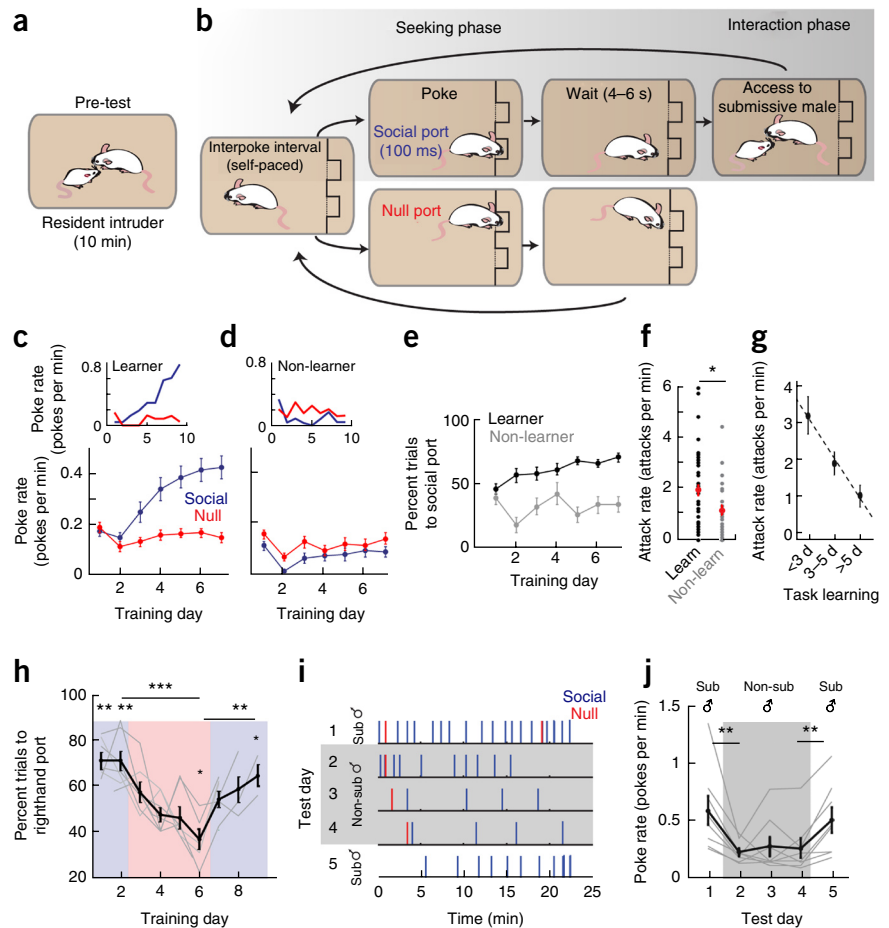
Individual mice did not learn this task equally (**Fig. 1c**–**e**). In 43 of 76 animals (learners, 56.6%), both the rate of trial initiation and the percentage of responses directed to the social port increased rapidly across days relative to the null port (**Fig. 1c**). These animals that showed rapid task learning were highly aggressive during this task, attacking the submissive male on vast majority of trials. On the final day of training, attacks occurred on 96.8 ± 5.5% (mean ± s.d.) of trials. In contrast, the remaining mice (33 of 76, non-learners, 43.4%) did not exhibit preference for the social port compared with the null port, and many (18 of 33) stopped poking the social port entirely by their final day of training (**Fig. 1d**). Across the total population, learners showed a steady increase in the preference for the social port, whereas non-learners did not show a preference (**Fig. 1e**).

Learners were more aggressive than non-learners during the resident intruder pre-test, exhibiting a significantly higher attack rate ($t(67) = 2.201$, $P = 0.031$, t test; **Fig. 1f**). In addition, among task learners, attack rates during the resident-intruder test were correlated with rates of task learning, such that more aggressive males exhibited faster task learning ($r = -0.410$, $P = 0.009$, $N = 39$ mice, robust regression; **Fig. 1g**). There was no indication that non-learners in the SIA task were compromised in their ability to learn the task contingency in general, given that they readily learned a similar task for a water reward (**Supplementary Fig. 1a**,**b**).

In learner males, using a series of control experiments, we found that the rates of trial initiation were contingent on attack opportunity. First,

response rates significantly decreased if access to the submissive male was terminated through extinction training ($t(9) = 2.988$, $P = 0.015$, paired t test, $N = 10$ mice; **Supplementary Fig. 1c**) or submissive males were presented in a perforated enclosure during the interaction phase to prevent attack ($t(6) = 2.694$, $P = 0.036$, paired t test, $N = 7$ mice; **Supplementary Fig. 1d**). Animals also readily reversed their port preference if the reinforcement contingency was reversed (**Fig. 1h**). Lastly, these trained males strongly preferred to initiate trials for access to highly defeated submissive males rather than non-submissive males who had not been defeated. When access to the submissive male was substituted with access to a non-submissive male, response rates in the SIA task declined significantly (between day 1 and 2, $t(7) = 3.548$, $P = 0.009$, paired t test, $N = 8$ mice; **Fig. 1i**,**j**). Higher rates of trial initiation were immediately recovered when access to a submissive male was resumed (between day 4 and 5, $t(7) = -4.167$, $P = 0.004$, paired t test, $N = 8$; **Fig. 1i**,**j**). These data demonstrate that animals were not motivated to perform the task purely for social reasons and were instead reinforced by the opportunity to attack and win.

VMHvl neurons are active during aggression seeking
VMHvl neurons are strongly activated by both male sensory cues and by attack itself[21,23], but whether neurons would be active during conspecific-independent aggression-seeking was unknown. To address this, we recorded the activity of populations of VMHvl neurons during the SIA task in fully trained male mice. A total of 169
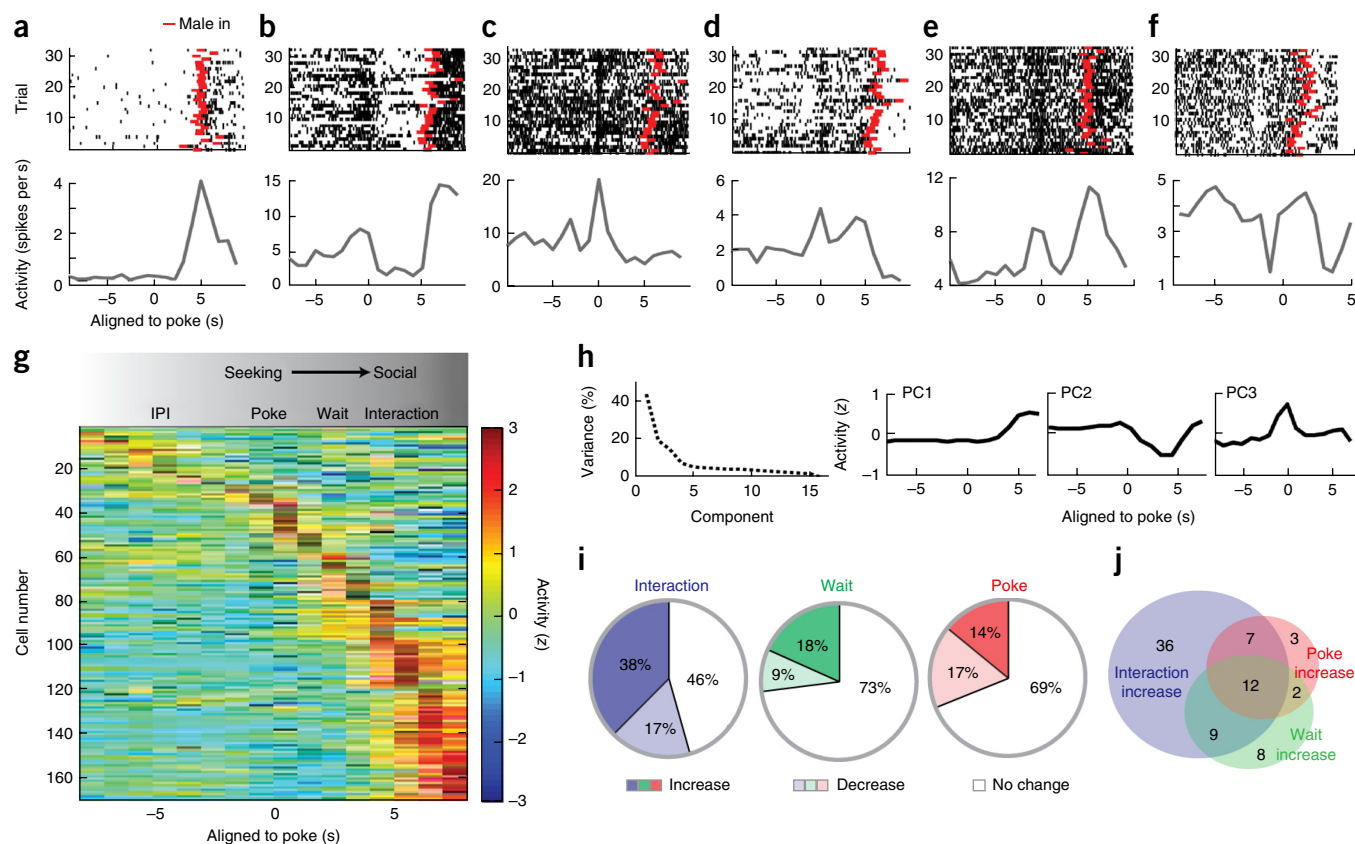
Figure 2 VMHvl neurons are modulated during aggression seeking, waiting and interaction phases. (**a**–**f**) Raster plots (top) and PETHs (bottom) of six representative neurons (6 of 169) aligned to the time of poke initiation showing peak responses during different task phases. Red ticks indicate the introduction of the submissive male for each trial. (**g**) Activity matrix of the total population sorted by the peak response time for each neuron ($n = 169$ cells in 3 mice). (**h**) Variance was explained (left) by the principal components of population activity matrix in **g**. PC1–3 (right) explained 60% of the total variance and corresponded to modulation during the interaction, wait and poke phases. (**i**) Percentage of neurons with activity significantly different from activity during the interpoke interval (IPI) ($n = 169$, within-neuron signed rank test with FDR correction, $P < 0.05$, poke bin: −1 s to 1 s around poke, wait bin: 1–3 s after poke, interaction bin: 0–3 s after male introduction, IPI bin: −15 to −1 s before poke). (**j**) Venn diagram of overlap between subpopulations with increased activity during interaction, wait and poke epochs. *$P < 0.05$, **$P < 0.01$, ***$P < 0.001$.

single units were recorded using a moveable, 16-channel microwire bundle in three animals in which electrode placement was confirmed histologically *post hoc* (**Supplementary Fig. 2a,b**).

We examined the temporal response profiles during the seeking and interaction phases of the SIA task by plotting spike rasters and peri-event time histograms (PETHs) of individual neurons aligned to the initiation of the nosepoke. Although some neurons responded exclusively during the interaction phase of the SIA task (**Fig. 2a**), many VMHvl neurons were also modulated at other distinct time points during the SIA task when the submissive male was not present, but as animals initiated a trial or waited for the introduction of the male (**Fig. 2b**–**f**). Sorting the population activity by neurons' peak response times revealed that the activity of a subpopulation of neurons peaked at the time of the nosepoke (time −1 s to 1 s around poke) or during the waiting period (1–3 s after poke), whereas the largest group of neurons was maximally active during the interaction phase of aggression (**Fig. 2g**). Principal components analysis (PCA) revealed that the first three components of the activity matrix (modulated during the interaction, wait and nosepoke, respectively) accounted for over 60% of the total population variance (**Fig. 2h**) and neurons could be grouped along similar dimensions (poke, wait and interaction) using an Ward's hierarchical agglomerative clustering method (**Supplementary Fig. 2c**).

A comparison of the trial-to-trial, within-neuron activity during the poke, wait and interaction epochs to the activity during the

interpoke interval revealed that approximately one-third (52 of 169) of the population was significantly modulated during the poke, over a quarter (46 of 169) was modulated during the wait and over half (93 of 169) were modulated during the interaction phase (Wilcoxon signed rank test with false discovery rate below 0.05 for each task epoch; **Fig. 2i**). Notably, neurons with increased activity during poke were significantly more likely to have an increased response during the interaction (19 of 24, Fisher's exact test, $P = 1.50 \times 10^{-5}$), indicating that a subset of attack-responsive cells were active during aggression seeking, even in the absence of conspecific sensory cues (**Fig. 2j**).

Population activity tracks task learning and extinction

To investigate how VMHvl responses during single trials evolved as the animals learned the relationship between poking and future attack, we used fiber photometry[26,27] to record VMHvl population activity as behavior changed during task learning and extinction[26,27]. We virally expressed the genetically encoded calcium indicator GCaMP6s[28] in the VMHvl of six untrained males. GCaMP6 expression was largely limited to the VMH with minor spread along the fiber track (**Fig. 3a**). *Post hoc* histological analysis revealed that 90% of GCaMP6-labeled neurons in the light cone below the fiber end were located in the VMHvl and at least 30% of the total number of VMHvl cells were labeled.

Beginning 3 weeks after viral injection, we performed daily recordings of the GCaMP6 signal using fiber photometry as the animals
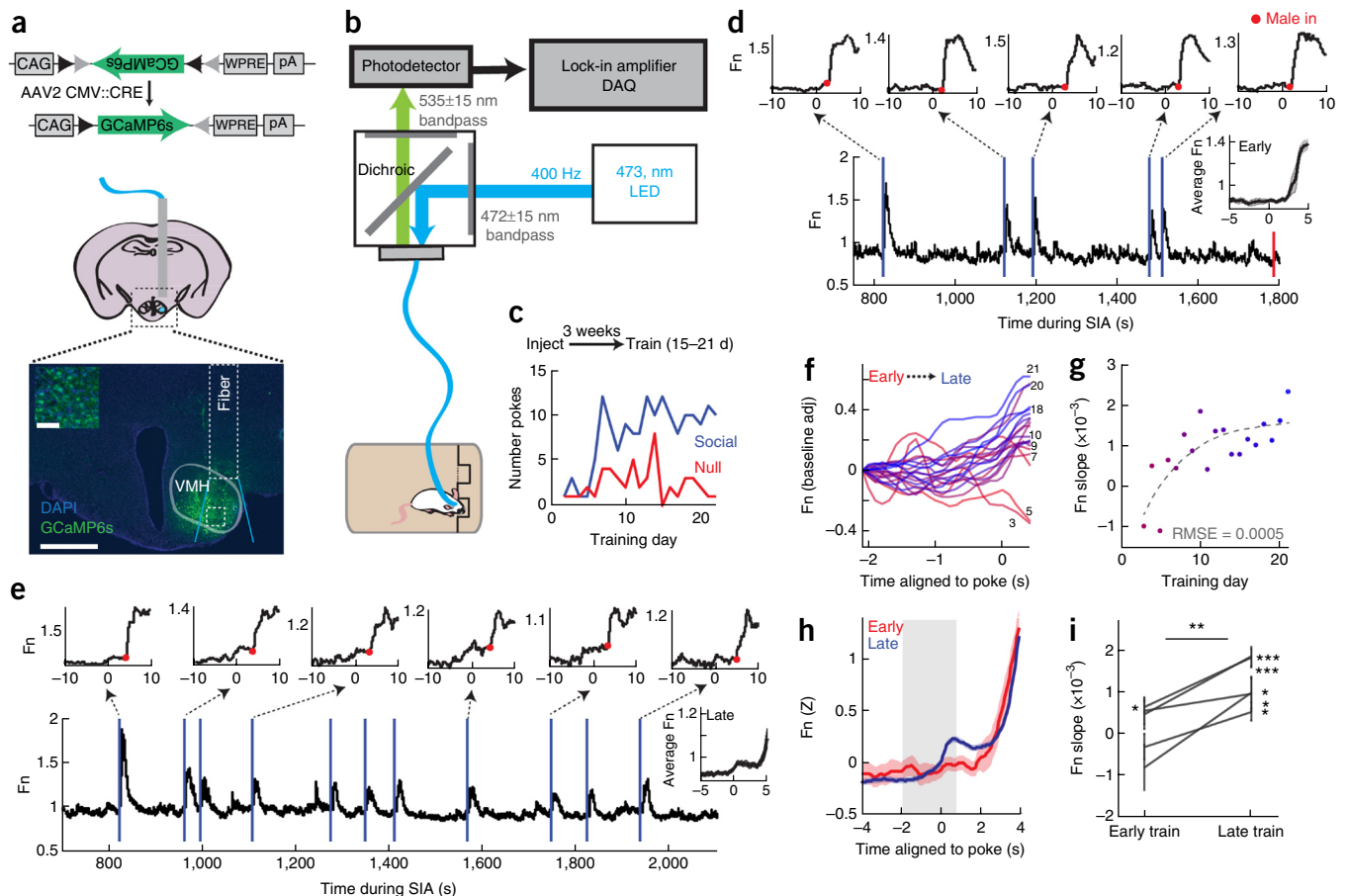
Figure 3 VMHvl population activity during aggression-seeking tracks task learning. (**a**) Viruses expressing GCaMP6 were injected before training. Histology shows a representative recording site with light cone. Inset, magnification of the boxed region. Scale bars represent 500 μm and 100 μm (inset). (**b**) Setup for fiber photometry. (**c**) Learning curve for representative animal (one of five mice) shown in **d**–**g**. GCaMP6 signal (Fn) during early (**d**) and late (**e**) training sessions for individual shown in **a** and **c**. Vertical lines indicate poke times for social (blue) and null (red). Insets, single-trial responses aligned to nosepokes. Red dots indicate male introduction. Right insets, mean poke-aligned response ± s.e.m. (**f**) Poke-aligned activity for all sessions for the animal shown in **c**–**e**. Shading shows transition from early (red) to late (blue) training days. Training day numbers are shown to the left of response curves. (**g**) Slopes of activity shown in **f** as a function of training day. Colors are as defined in **f**. Dotted line shows best fitting curve (root-mean-square error, RMSE). (**h**) Population activity aligned to poke from early training trials (first 4 d, red) and late training trials (last 4 d, blue). $N = 5$ mice. (**i**) Mean response slope (-2–0.5 s around poke, gray bar shown in **h**) for early and late trials ($P = 0.009$, paired t test, $N = 5$ mice). Data are presented as mean ± s.e.m. within-animal trials (for late training slope distributions in each animal: $t(41) = 9.185$, $P = 1.67 \times 10^{-11}$, $n = 42$ trials; $t(39) = 7.2428$, $P = 9.97 \times 10^{-9}$, $n = 40$ trials; $t(41) = 2.314$, $P = 0.026$, $n = 42$ trials; $t(37) = 2.438$, $P = 0.020$, $n = 38$ trials; $t(77) = 2.552$, $P = 0.013$, $n = 78$ trials; t test). *$P < 0.05$, **$P < 0.01$, ***$P < 0.001$.

were trained on the SIA task[26,27] (**Fig. 3b,c**). Of six injected animals, five met task learning criteria. In these animals, we found that, early in task training, when poke rates were low and animals showed weak or no bias toward the social port, GCaMP6 signal increased after the introduction of the male, but showed little increase at the time of the poke (**Fig. 3d**). In contrast, during late training, where animals exhibited clear task learning and strong behavioral bias toward the social port, activity in single trials showed a robust increase during the seeking and waiting phases before male introduction (**Fig. 3e** and **Supplementary Video 1**). We analyzed activity slope during the seeking phase of the task (-2 s to 0.5 s around poke) and examined its relationship to task learning. Activity slopes during seeking increased substantially as a function of training day (**Fig. 3f,g**), with consistent positive values in individuals emerging only after animals showed a clear bias toward the social port (**Fig. 3g**). Across the population of task-trained animals (**Fig. 3h,i**), we found that mean slopes fit to single trials in individual animals during early training (first 4 d) were largely unbiased in sign, whereas, during late training, activity

from each animal showed a clear bias for positive slopes during the seeking phase (for animals 1–5: $t(41) = 9.185$, $P = 1.67 \times 10^{-11}$, $n = 42$ trials; $t(39) = 7.2428$, $P = 9.97 \times 10^{-9}$, $n = 40$ trials; $t(41) = 2.314$, $P = 0.026$, $n = 42$ trials; $t(37) = 2.438$, $P = 0.020$, $n = 38$ trials; $t(77) = 2.552$, $P = 0.013$, $n = 78$ trials; t test). The mean slopes for activity in the aggression seeking phase were significantly increased during late training compared with early training ($t(4) = -4.740$, $P = 0.009$, $N = 5$ mice, paired t test) in animals that successfully learned the task. In contrast, no consistent effect in slope was observed in a GCamP6-expressing animal that was recorded, but did not meet task learning criteria (**Supplementary Fig. 3**).

We next tested whether activity in the VMHvl would track changes in behavior during task extinction. In the five trained GCaMP6s-expressing animals that met task learning criteria, we recorded VMHvl population activity during two successive days of extinction, when nosepoking was no longer reinforced by access to the submissive male (**Fig. 4a**). Behaviorally, after a period of initial perseveration, poke rates decreased (**Fig. 4b**) and were accompanied by a decrease in
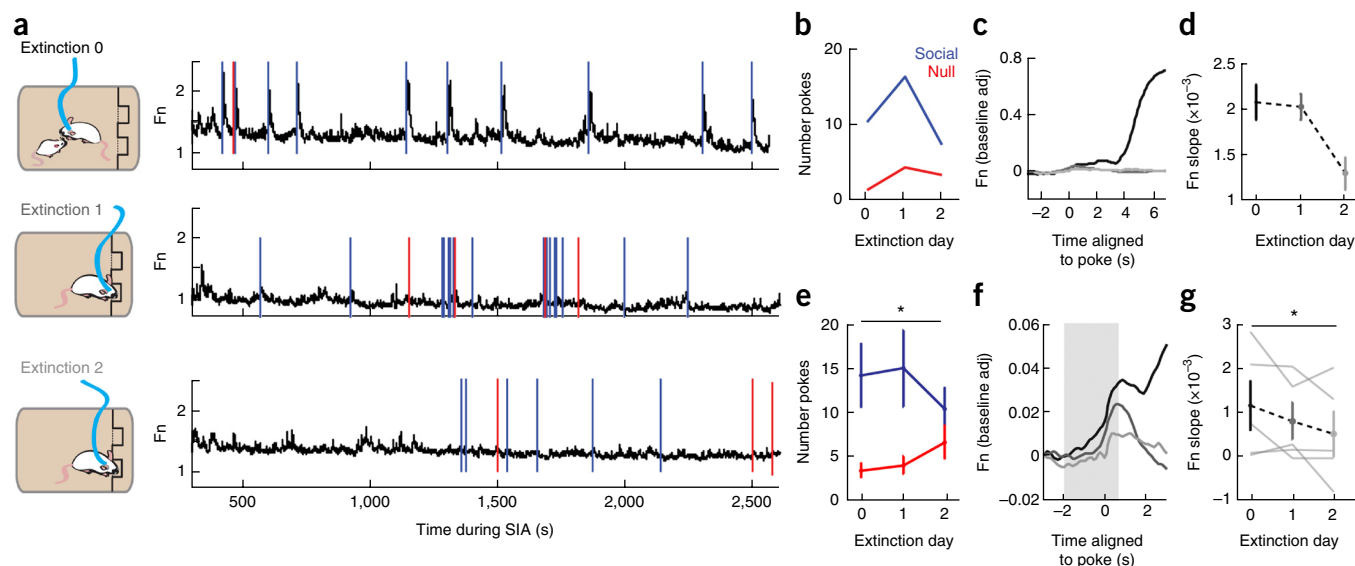
Figure 4 VMHvl population activity decreases during extinction. (**a,b**) GCaMP6 activity (**a**) and behavior (**b**) shown for final day of SIA training (extinction day 0, top) and two consecutive days of extinction training for representative animal (one of five). Blue and red ticks represent pokes to social and null ports, respectively. Animal showed behavioral perseveration on extinction day 1 followed by a reduction in response rate on extinction day 2. (**c**) Mean poke-aligned response for extinction day 0 (black) and during extinction training (extinction days 1–2, gray). (**d**) Slopes of population response during seeking (gray bar in **f**) for extinction days 0–2. (**e**) Response to social port decreased in extinction day 2 relative to extinction day 0 ($t(4) = 2.881$, $P = 0.045$, paired t test, extinction day 0 versus extinction day 2, $N = 5$ mice). (**f**) Averaged poke-aligned responses during extinction days 0–2 ($N = 5$ mice). (**g**) Mean poke-aligned response slope (-2–0.5 s around poke, gray bar, **f**) decreased for extinction day 2 relative to extinction day 0 ($t(4) = 3.352$, $P = 0.029$, paired t test, $N = 5$ mice). In **d**, **e** and **g**, data are presented as mean ± s.e.m. $*P < 0.05$, $**P < 0.01$, $***P < 0.001$.

activity slope around the time of the poke (**Fig. 4c,d**). These effects on behavior ($t(4) = 2.881$, $P = 0.045$, paired t test, extinction day 0 versus extinction day 2, $N = 5$ mice; **Fig. 4e**) and activity slope ($t(4) = 3.352$, $P = 0.029$; **Fig. 4f,g**) were significant across animals.

To test whether activity changes during aggression seeking were present in an early sensory relay upstream of the VMHvl, we recorded GCaMP6s activity in the main olfactory bulb (MOB) during the SIA training ($N = 2$ mice; **Supplementary Fig. 4**). While activity in the MOB increased during investigation of male and female intruders (**Supplementary Fig. 4b,c**) and fluctuated at the respiratory rate of mouse (**Supplementary Fig. 4d,e**), we observed a decrease rather than an increase in activity at the time of the nosepoke after SIA task training, supporting a lack of olfactory input during aggression seeking in our task design (**Supplementary Fig. 4f–l**). Lastly, we observed little to no change in fluorescence in animals expressing GFP in the VMHvl during aggressive behavior (**Supplementary Fig. 5**), indicating that the contribution of movement-induced artifacts to the fluorescent signal was negligible.

VMHvl inactivation reduces aggression-seeking behavior

The VMHvl is critical for the expression of aggressive action[20–22], but its functional role in aggression-seeking behavior has not been explored. To explore this directly, we virally expressed a G_i-coupled designer receptor exclusively activated by designer drug (DREADDi) conjugated with red fluorescent protein mCherry bilaterally in the VMHvl of a population of animals trained on the SIA task (**Fig. 5a,b**). DREADDi is an engineered receptor that hyperpolarizes neurons following binding to its synthetic ligand clozapine-N-oxide (CNO)[29]. *Post hoc* histological analysis showed that DREADDi-mCherry–expressing neurons in all animals were centered between the median and posterior VMHvl in all animals and therefore no animals were excluded from analysis ($N = 6$ mice; **Fig. 5a** and **Supplementary Fig. 6a**). During surgery, animals were also implanted with chronic electrodes

for electromyography (EMG) in the superficial masseter muscle of the jaw to quantify accurate attack timing and biting intensity[30,31].

Systemic injections of CNO in all animals reduced the attack time and the number of putative-bite events detected by EMG during a resident-intruder test ($t(5) = 5.663$, $P = 0.002$, paired t test; $P = 0.031$, Wilcoxon signed rank test, $N = 6$; **Fig. 5c,d**), confirming that DREADDi inactivation targeted aggression-relevant neurons. We next examined the effect of VMHvl inactivation on the performance in the SIA task by alternating between injections of saline and CNO (1 mg per kg of body weight) across four consecutive days. We found that CNO injections significantly reduced poke rates for the social port within individuals (**Fig. 5e**) and across all animals (center, $F_{3,15} = 8.51$, $P = 0.002$, repeated-measures ANOVA; **Fig. 5f**), but did not affect poke rates to the null port (right, $F_{3,15} = 0.02$, $P = 0.997$, repeated-measures ANOVA; **Fig. 5f**). CNO-mediated inactivation did not induce motor impairment during this task: neither the spontaneous locomotion of the animals nor their performance on a rotarod test was affected during CNO-treated days relative to saline treated days (**Supplementary Fig. 6b,c**). CNO administration in no virus–injected control mice did not affect attack rate or putative-bite rate during a resident-intruder test ($t(3) = 0.344$, $P = 0.753$ attack rate; $t(3) = 0.881$, $P = 0.443$; EMG detected bite events, paired t test, $N = 4$ mice). As further confirmation of our pharmacogenetic inactivation, injections of muscimol, a GABA$_A$ receptor agonist, into the VMHvl area were also sufficient to reduce poke rates during the SIA task (**Supplementary Fig. 6d–f**).

To test whether inactivation effects were specific to the SIA task in which animals poked for access to a submissive male, we retrained the same DREADDi-expressing males to nose poke for a water reward. We found that CNO-mediated VMHvl inactivation did not reduce the poke rate for either water-port or null-port relative to the saline control injection (water-port poke rate: $F_{3,15} = 1.663$, $P = 0.218$; null-port poke rate: $F_{3,15} = 1.815$, $P = 0.188$; repeated-measures ANOVA; **Fig. 5g**).
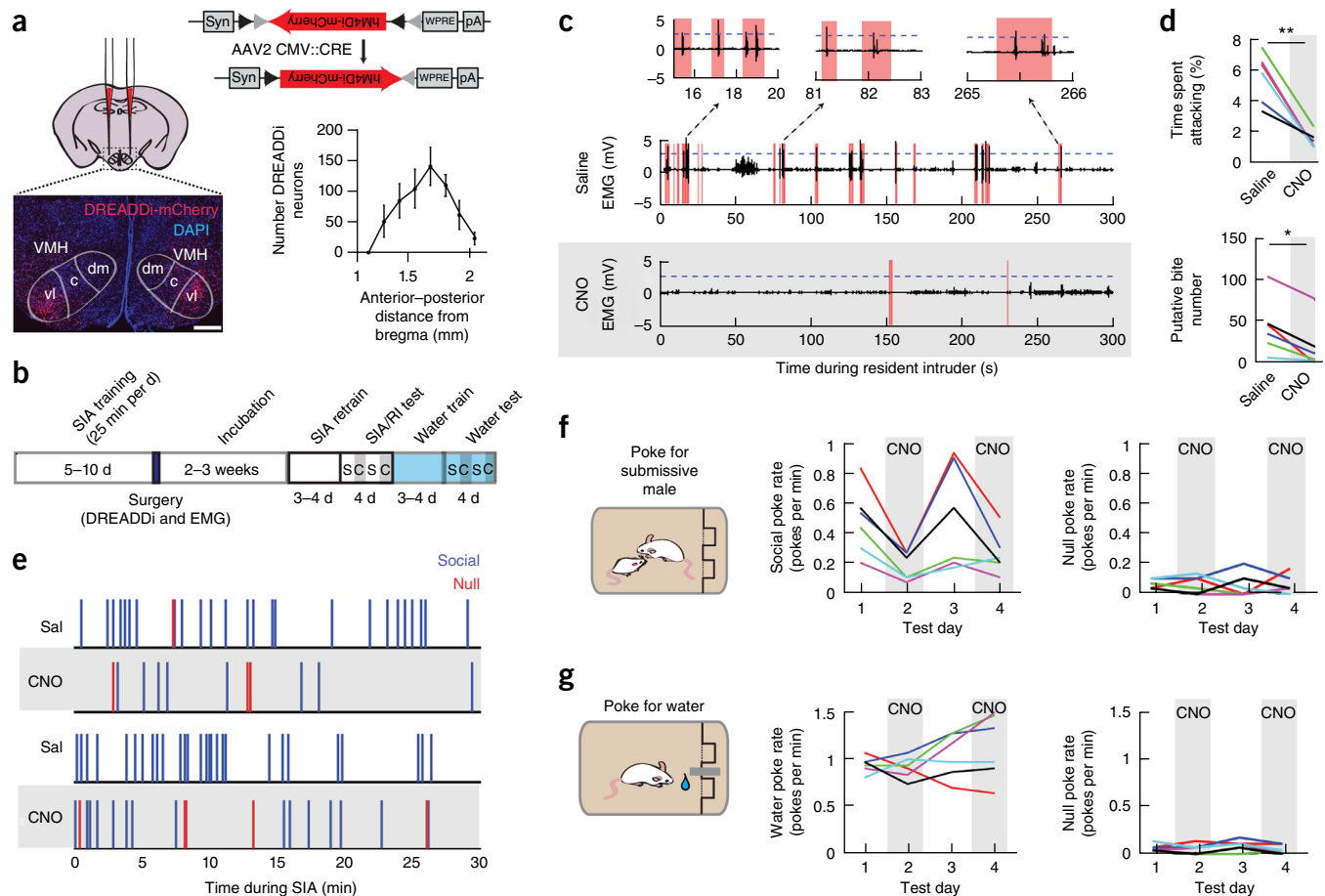
Figure 5 Reversible pharmacogenetic inactivation of VMHvl reduces aggression-seeking behavior. (**a**) Task-trained learner males were injected bilaterally into the VMHvl with virally expressed DREADD G_i. Expression of DREADDi-mCherry in a representative coronal section is shown. Scale bar represents 250 μm. The average numbers of DREADDi-infected neurons in the VMHvl are plotted. Data are presented as mean ± s.e.m. (**b**) Sequence of training, surgery and testing. Alternating white or blue and gray bars show saline- and CNO-injection days, respectively. (**c**) Representative jaw EMG traces (one of six mice) for the resident-intruder test after saline (top) or CNO intraperitoneal injection (bottom) (red, attacks; dashed lines EMG bite threshold). (**d**) Reduced aggression in the resident-intruder assay (top, $t(5) = 5.663$, $P = 0.002$, paired t test) and fewer EMG-detected putative-bites following CNO injections compared with saline injections (bottom, $P = 0.031$, Wilcoxon signed rank test, $N = 6$ mice). (**e**) Example behavior during the SIA task following saline (white) and CNO (gray) injections (one of six mice). (**f**) Reduced rates of poking for the social port following CNO injection (correct: $F_{3,15} = 8.51$, $P = 0.0015$, repeated-measures ANOVA) without significantly altering the null poke rate ($F_{3,15} = 0.02$, $P = 0.997$). (**g**) No reduction in poking after CNO for a water reward (water response, $F_{3,15} = 1.663$, $P = 0.218$; null response, $F_{3,15} = 1.815$, $P = 0.188$; repeated-measures ANOVA). $N = 6$ mice in **d**, **f** and **g**. Each color in **d**, **f** and **g** represents one animal. $*P < 0.05$, $**P < 0.01$, $***P < 0.001$.

Optogenetic stimulation accelerates aggression seeking

We next tested whether activation of VMHvl neurons during the interpoke interval could acutely promote aggression-seeking behavior and bias animals toward shorter poke initiation latencies. We virally expressed channelrhodopsin (ChR2, ref. 32) in the VMHvl bilaterally in a population of males trained on the SIA task (**Fig. 6a**) and implanted a light delivery cannula over each injection site (**Supplementary Fig. 7**). To ensure that ChR2 was expressed in aggression-related cells, we screened for functional sites from which high-frequency light stimulation was sufficient to evoke attack toward a castrated male, a social stimulus that normally evokes little spontaneous attack during resident-intruder test (10–20 Hz, 10 ms, 0.5–1.5 mW; **Supplementary Fig. 8a–c**)[21]. In 18 sites from 9 animals, we identified 7 functional sites in 6 animals (left VMHvl, functional site; right VMHvl, non-functional site; **Fig. 6a**). In the remaining tested sites (11 of 18), stimulation either induced no behavioral change or evoked defense-like responses including avoidance, cornering and freezing (**Supplementary Fig. 8d**).

We next delivered low-frequency light pulses (5–10 Hz, 10 ms) to functional VMHvl sites during the interpoke interval of the SIA task, alternating between within-session 'real' and sham (0 mW) stimulation trials (**Fig. 6b**). During each trial, stimulation was terminated automatically following the initiation of the nosepoke and animals were not stimulated during the social interactions themselves. After each interaction, real or sham stimulation was re-initiated after the removal of the submissive male. We found that mean poke latencies were significantly and consistently reduced during stimulation trials compared with sham stimulation trials during each of three test sessions across animals ($t(6) = 3.337$, $P = 0.016$; $t(6) = 2.507$, $P = 0.046$; $t(6) = 3.438$, $P = 0.014$ for each of three test sessions, $N = 7$ sites, paired t test; **Fig. 6c–e** and **Supplementary Video 2**). Stimulation did not result in an increase in nonspecific poking to the null port. Although the animals were not stimulated during the interaction phase of the SIA task, interactions following real stimulation contained a higher frequency of putative bites than interactions following sham stimulation ($t(5) = -5.451$, $P = 0.003$, paired t test; **Fig. 6f,g**). Together,

Figure 6 Optogenetic stimulation of VMHvl accelerates aggression seeking by reducing poke latency. (**a**) Schematic of ChR2-EYFP expression and a representative histological image (below) showing the expression of ChR2-EYFP at a 'functional' site (left VMHvl) and a 'non-functional' site (right VMHvl). Scale bar represents 250 μm. (**b**) Animals were screened for functional sites by testing for stimulation-evoked behavior toward a castrated male. Sites that elicited stimulation-evoked attack were considered to be functional. Animals with functional sites were stimulated during the interpoke interval of the SIA task. (**c**,**d**) Stimulation (blue) decreased trial-to-trial poke initiation latency relative to sham stimulation (gray). Representative behavior from one of seven sites in six mice. (**e**) Stimulation reduces mean poke latency across days of testing ($N = 7$ sites, $t(6) = 3.337$, $P = 0.016$; $t(6) = 2.507$, $P = 0.046$; $t(6) = 3.438$, $P = 0.014$ for each of three test sessions). (**f**) Representative jaw EMG trace during SIA task. Dashed line shows threshold. (**g**) Putative-bite rate increases following stimulation trials ($t(5) = -5.451$, $P = 0.003$, paired t test. $N = 6$ sites). In **e** and **g**, data are presented as mean ± s.e.m. *$P < 0.05$, **$P < 0.01$, ***$P < 0.001$.
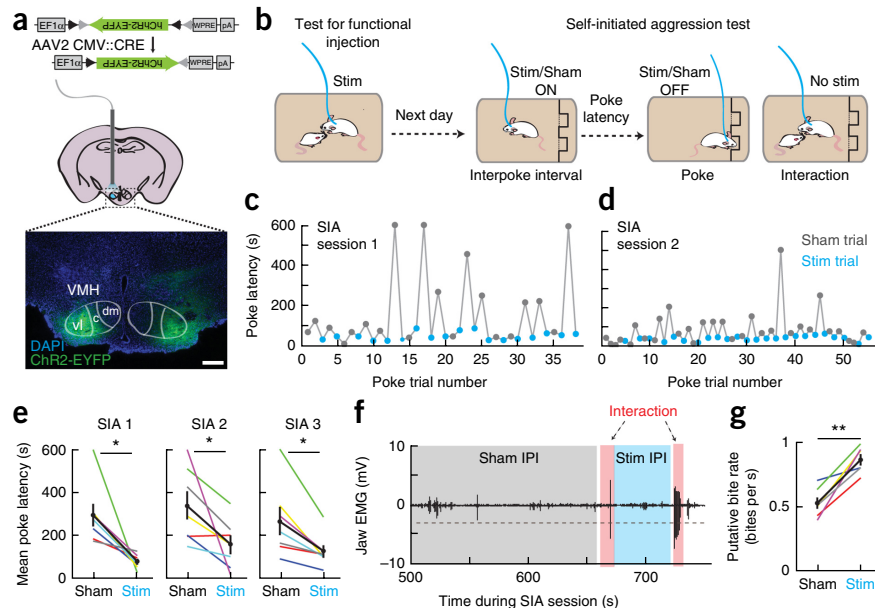
these findings indicate that stimulation not only accelerated aggression-seeking behavior, but also increased aggression intensity during interactions following these trials.

For non-functional sites, we observed no significant difference between the poke latencies of real and sham stimulation trials ($t(10) = -1.764$, $P = 0.102$, paired t test, $N = 11$ sites in 9 mice, **Supplementary Fig. 8e,f**). To control for the remote possibility that animals learned to switch off a potentially aversive stimulation by nosepoking during the SIA task, we tested whether animals would avoid stimulation using a real-time place preference (RTPP) test[33]. We did not observe any significant or systematic avoidance or preference for the stimulation chamber ($F_{2,7} = 1.05$, $P = 0.3752$, repeated-measures ANOVA, $N = 8$ mice, **Supplementary Fig. 8g,h**).

Lastly, in a separate set of animals, we tested whether VMHvl activation would affect behavior during a breakpoint assay, a classic test that quantifies motivation by assessing the amount of work an individual is willing to exert for a given reinforcement (**Supplementary Fig. 9a–c**)[2]. Each animal was first trained on the original SIA task, and, if the animal reached the learning criteria, a progressive-ratio schedule with a step size of 2 (PR2) was implemented to establish the breakpoint of the animal (**Supplementary Fig. 9d**). We found that optogenetic stimulation of the VMHvl significantly increased the behavioral breakpoint of these animals compared with a control sham stimulation test ($t(5) = -2.803$, $P = 0.038$, $N = 6$ functional sites in 5 mice, paired t test; **Supplementary Fig. 9e,f**). In tandem with the effects of stimulation during the SIA task, these results indicate that activation of the VMHvl not only accelerated the aggression-seeking behavior, but also increased the amount of work the animals would do for the opportunity to fight.

DISCUSSION

Here we describe our use of an aggression operant task to probe the neural correlates of moment-to-moment aggressive motivation. In this task, male mice repeatedly self-initiate trials to seek out opportunities to attack. Using this task, we identified the VMHvl as an essential region for aggressive motivation that is able to drive aggression-seeking behavior independent of aggression-provoking cues.

We found that neural activity in the VMHvl undergoes learning-dependent changes that serve to link a socially neutral behavior (the nosepoke) with the potential for future aggression. This activity change is functionally relevant such that bi-directional modulation of VMHvl activity was able to change the frequency and latency of this seeking behavior as well as the intensity of future attack. These results suggest that the VMHvl encodes aggression-predictive information not only during reactive aggression[23], but also during proactive aggression. The source of these predictive signals is not known and is likely multifaceted. The VMHvl is embedded in a complex network of inputs, including, but not limited to, intra-hypothalamic input from the medial preoptic area and the ventral part of the premammillary nucleus, and extra-hypothalamic input from bed nucleus of the stria terminalis, the lateral septum, cortical and medial amygdala, and ventral subiculum. Several of these areas have been previously implicated in mediating conspecific attack. In particular, optogenetic activation of GABAergic cells in the medial amygdala is sufficient to evoke attack in male mice, whereas either suppressing the activity of these GABAergic cells or killing aromatase-expressing cells in the medial amygdala decreases attack[34,35]. Electrophysiological recording also revealed the presence of conspecific odor–responsive cells in the medial amygdala[36]. However, as aggression-relevant medial amygdala neurons that project to the VMHvl are primarily inhibitory[37], their relationship to activity in the VMHvl is not yet clear. The nucleus accumbens and associated reward circuitry may also carry information about aggressive motivation or the rewarding aspect of aggression. Microdialysis experiments in the nucleus accumbens in aggressive males has shown that dopamine levels increase before an anticipated fight and can remain elevated during and after a single fight[38]. Although the nucleus accumbens does not project to the VMHvl directly, its information could potentially be relayed to the VMHvl through the medial preoptic area, a region that has been implicated in a variety of social behaviors.

Changes in circulating hormones in the VMHvl are also likely to have an effect on aggression-seeking behaviors and may facilitate task learning. A well-documented behavior is the 'winner-loser effect', which demonstrates a link between winning a competitive

event and a surge in testosterone. This surge then promotes further winning or other dominance seeking behaviors[39,40]. In our task, we observed a behavioral correlate of this effect, as animals increased seeking behavior for a submissive male when winning was assured and markedly reduced their rate of trial initiation for access to a non-submissive male, where winning was uncertain. Although animals were engaged in task learning for the submissive male, it is likely that these easily won fights triggered repeated surges of testosterone. As both androgen and estrogen receptors are highly enriched in the VMHvl, testosterone, after conversion to estrogen by local aromatase, could act through these receptors to trigger a cascade of molecular events[41]. These events may lead to changes in synaptic plasticity, which could modulate responses of VMHvl cells to specific upstream or local inputs and ultimately alter the propensity to engage in aggression-related behaviors[42,43]. Although increases in winning-related circulating testosterone may be essential for task learning and/or synaptic or circuit reorganization, it is less likely that increased circulating hormones have a direct causal role in generating the acute activity changes in VMHvl cell activity during nosepoking, given the slow timescale of these genomic effects (minutes to hours to days). However, there may be additional facilitating 'non-classical' effects of brain-derived estrogens that operate through membrane bound G-coupled protein receptors at faster timescales[44,45].

Although our results demonstrate that the VMHvl is not essential for the execution of a nonsocial seeking task (for a water reward), they do not rule out a potential role for the VMHvl in other social or sexual seeking behaviors. Low-intensity optogenetic activation of cells that express estrogen receptor alpha (ERα) in the VMHvl of male mice has been reported to induce approach and mounting behaviors in male mice[20], and electrophysiological recording revealed that a small portion of VMHvl cells increase in activity during female investigation, although not during advanced sexual intercourse[21,46]. In males, the identities of these female-responsive neurons partially overlap with the identities of male responsive neurons[21,46]. In addition, both knock-down of ERα[47] and genetic ablation of progesterone receptor–expressing neurons[22] in the VMHvl can cause deficits in male sexual behavior. Although the effects that we observed appeared to be specific to aggression (that is, stimulation does not promote sexual behaviors toward the submissive male during this task), future studies may address whether the VMHvl is also involved in sexual seeking behaviors, either through discrete or partially overlapping local circuitry.

Recent studies in the lateral hypothalamus have shown that GABAergic cells are active during both pursuit and consumption of food[48]. Here, we found an analogous role of the hypothalamus for a socially motivated behavior: VMHvl cells were active during both aggression-seeking and attack. These results support a role for the hypothalamus in not only initiating species specific 'consummatory' actions such as feeding or attack, but also signaling the 'appetitive' or motivational state of the animal and flexibly driving appropriate motor actions to obtain the corresponding target. Mice, humans and other vertebrates vary considerably in the expression of aggressive action, yet hypothalamic neural circuitry remains largely conserved across these species[15,49,50], suggesting that multiple modes of aggressive action may emerge from a common motivational mechanism. Our data provide new evidence of a neural substrate for aggressive motivation and offer insight into the neural processes that mediate goal-directed social behaviors.

METHODS

Methods and any associated references are available in the online version of the paper.

1. Fish, E.W., De Bold, J.F. & Miczek, K.A. Aggressive behavior as a reinforcer in mice: activation by allopregnanolone. *Psychopharmacology (Berl.)* **163**, 459–466 (2002).
2. May, M.E. & Kennedy, C.H. Aggression as positive reinforcement in mice under various ratio- and time-based reinforcement schedules. *J. Exp. Anal. Behav.* **91**, 185–196 (2009).
3. Van Hemel, P.E. Aggression as a reinforcer: operant behavor in the mouse-killing rat. *J. Exp. Anal. Behav.* **17**, 237–245 (1972).
4. Turnbough, P.D. & Lloyd, K.E. Operant responding in Siamese fighting fish (*Betta splendens*) as a function of schedule of reinforcement and visual reinforcers. *J. Exp. Anal. Behav.* **20**, 355–362 (1973).
5. Azrin, N.H., Hutchinson, R.R. & McLaughlin, R. The opportunity for aggression as an operant reinforcer during aversive stimulation. *J. Exp. Anal. Behav.* **8**, 171–180 (1965).
6. Bannai, M., Fish, E.W., Faccidomo, S. & Miczek, K.A. Anti-aggressive effects of agonists at 5-HT1B receptors in the dorsal raphe nucleus of mice. *Psychopharmacology (Berl.)* **193**, 295–304 (2007).
7. Couppis, M.H. & Kennedy, C.H. The rewarding effect of aggression is reduced by nucleus accumbens dopamine receptor antagonism in mice. *Psychopharmacology (Berl.)* **197**, 449–456 (2008).
8. de Almeida, R.M., Nikulina, E.M., Faccidomo, S., Fish, E.W. & Miczek, K.A. Zolmitriptan—a 5-HT1B/D agonist, alcohol, and aggression in mice. *Psychopharmacology (Berl.)* **157**, 131–141 (2001).
9. Fish, E.W., DeBold, J.F. & Miczek, K.A. Escalated aggression as a reward: corticosterone and GABA(A) receptor positive modulators in mice. *Psychopharmacology (Berl.)* **182**, 116–127 (2005).
10. Crowcroft, P. *Mice All Over* (Foulis, 1966).
11. Mitani, J.C., Watts, D.P. & Amsler, S.J. Lethal intergroup aggression leads to territorial expansion in wild chimpanzees. *Curr. Biol.* **20**, R507–R508 (2010).
12. Nelson, R.J. & Trainor, B.C. Neural mechanisms of aggression. *Nat. Rev. Neurosci.* **8**, 536–546 (2007).
13. Blair, R.J. Neurocognitive models of aggression, the antisocial personality disorders and psychopathy. *J. Neurol. Neurosurg. Psychiatry* **71**, 727–731 (2001).
14. Martínez, M., Guillén-Salazar, F., Salvador, A. & Simón, V.M. Successful intermale aggression and conditioned place preference in mice. *Physiol. Behav.* **58**, 323–328 (1995).
15. O'Connell, L.A. & Hofmann, H.A. Evolution of a vertebrate social decision-making network. *Science* **336**, 1154–1157 (2012).
16. Lammers, J.H., Kruk, M.R., Meelis, W. & van der Poel, A.M. Hypothalamic substrates for brain stimulation-induced attack, teeth-chattering and social grooming in the rat. *Brain Research* **449**, 311–327 (1988).
17. Lipp, H.P. & Hunsperger, R.W. Threat, attack and flight elicited by electrical stimulation of the ventromedial hypothalamus of the marmoset monkey Callithrix jacchus. *Brain Behav. Evol.* **15**, 260–293 (1978).
18. Siegel, A. & Pott, C.B. Neural substrates of aggression and flight in the cat. *Prog. Neurobiol.* **31**, 261–283 (1988).
19. Siegel, A., Roeling, T.A.P., Gregg, T.R. & Kruk, M.R. Neuropharmacology of brain-stimulation-evoked aggression. *Neurosci. Biobehav. Rev.* **23**, 359–389 (1999).
20. Lee, H. *et al.* Scalable control of mounting and attack by Esr1+ neurons in the ventromedial hypothalamus. *Nature* **509**, 627–632 (2014).
21. Lin, D. *et al.* Functional identification of an aggression locus in the mouse hypothalamus. *Nature* **470**, 221–226 (2011).

22. Yang, C.F. *et al.* Sexually dimorphic neurons in the ventromedial hypothalamus govern mating in both sexes and aggression in males. *Cell* **153**, 896–909 (2013).
23. Falkner, A.L., Dollar, P., Perona, P., Anderson, D.J. & Lin, D. Decoding ventromedial hypothalamic neural activity during male mouse aggression. *J. Neurosci.* **34**, 5971–5984 (2014).
24. Haaren, F.v. *Methods in Behavioral Pharmacology* (Elsevier, 1993).
25. Koolhaas, J.M. *et al.* The resident-intruder paradigm: a standardized test for aggression, violence and social stress. *J. Vis. Exp.* **4367**, e4367 10.3791/4367 (2013).
26. Gunaydin, L.A. *et al.* Natural neural projection dynamics underlying social behavior. *Cell* **157**, 1535–1551 (2014).
27. Cui, G. *et al.* Concurrent activation of striatal direct and indirect pathways during action initiation. *Nature* **494**, 238–242 (2013).
28. Chen, T.W. *et al.* Ultrasensitive fluorescent proteins for imaging neuronal activity. *Nature* **499**, 295–300 (2013).
29. Dong, S., Rogan, S.C. & Roth, B.L. Directed molecular evolution of DREADDs: a generic approach to creating next-generation RASSLs. *Nat. Protoc.* **5**, 561–573 (2010).
30. Lippold, O.C.J. The relation between integrated action potentials in a human muscle and its isometric tension. *J. Physiol. (Lond.)* **117**, 492–499 (1952).
31. Hidaka, O. *et al.* Regulation of masticatory force during cortically induced rhythmic jaw movements in the anesthetized rabbit. *J. Neurophysiol.* **77**, 3168–3179 (1997).
32. Boyden, E.S., Zhang, F., Bamberg, E., Nagel, G. & Deisseroth, K. Millisecond-timescale, genetically targeted optical control of neural activity. *Nat Neurosci* **8**, 1263–1268 (2005).
33. Stamatakis, A.M. & Stuber, G.D. Activation of lateral habenula inputs to the ventral midbrain promotes behavioral avoidance. *Nat. Neurosci.* **15**, 1105–1107 (2012).
34. Hong, W., Kim, D.W. & Anderson, D.J. Antagonistic control of social versus repetitive self-grooming behaviors by separable amygdala neuronal subsets. *Cell* **158**, 1348–1361 (2014).
35. Unger, E.K. *et al.* Medial amygdalar aromatase neurons regulate aggression in both sexes. *Cell Reports* **10**, 453–462 (2015).
36. Bergan, J.F., Ben-Shaul, Y. & Dulac, C. Sex-specific processing of social cues in the medial amygdala. *Elife* **3** doi:10.7554/eLife.02743 (2014).
37. Choi, G.B. *et al.* Lhx6 delineates a pathway mediating innate reproductive behaviors from the amygdala to the hypothalamus. *Neuron* **46**, 647–660 (2005).
38. Ferrari, P.F., van Erp, A.M., Tornatzky, W. & Miczek, K.A. Accumbal dopamine and serotonin in anticipation of the next aggressive episode in rats. *Eur. J. Neurosci.* **17**, 371–378 (2003).
39. Bernstein, I.S., Rose, R.M. & Gordon, T.P. Behavioral and environmental events influencing primate testosterone levels. *J. Hum. Evol.* **3**, 517–525 (1974).
40. Fuxjager, M.J., Oyegbile, T.O. & Marler, C.A. Independent and additive contributions of postvictory testosterone and social experience to the development of the winner effect. *Endocrinology* **152**, 3422–3429 (2011).
41. Simerly, R.B., Chang, C., Muramatsu, M. & Swanson, L.W. Distribution of androgen and estrogen receptor mRNA-containing cells in the rat brain: an in situ hybridization study. *J. Comp. Neurol.* **294**, 76–95 (1990).
42. Raskin, K. *et al.* Conditional inactivation of androgen receptor gene in the nervous system: effects on male behavioral and neuroendocrine responses. *J. Neurosci.* **29**, 4461–4470 (2009).
43. McEwen, B.S. *et al.* Steroid hormones as mediators of neural plasticity. *J. Steroid Biochem. Mol. Biol.* **39**, 223–232 (1991).
44. Roepke, T.A., Ronnekleiv, O.K. & Kelly, M.J. Physiological consequences of membrane-initiated estrogen signaling in the brain. *Front. Biosci. (Landmark Ed.)* **16**, 1560–1573 (2011).
45. Micevych, P.E. & Mermelstein, P.G. Membrane estrogen receptors acting through metabotropic glutamate receptors: an emerging mechanism of estrogen action in brain. *Mol. Neurobiol.* **38**, 66–77 (2008).
46. Falkner, A.L. & Lin, D. Recent advances in understanding the role of the hypothalamic circuit during aggression. *Front. Syst. Neurosci.* **8**, 168 (2014).
47. Sano, K., Tsuda, M.C., Musatov, S., Sakamoto, T. & Ogawa, S. Differential effects of site-specific knockdown of estrogen receptor α in the medial amygdala, medial pre-optic area, and ventromedial nucleus of the hypothalamus on sexual and aggressive behavior of male mice. *Eur. J. Neurosci.* **37**, 1308–1319 (2013).
48. Jennings, J.H. *et al.* Visualizing hypothalamic network dynamics for appetitive and consummatory behaviors. *Cell* **160**, 516–527 (2015).
49. Swanson, L.W. Cerebral hemisphere regulation of motivated behavior. *Brain Research* **886**, 113–164 (2000).
50. Toni, R., Malaguti, A., Benfenati, F. & Martini, L. The human hypothalamus: a morpho-functional perspective. *J. Endocrinol. Invest.* **27** (suppl.) 73–94 (2004).

ONLINE METHODS

Animals. Mice used for training on the SIA task and as the non-submissive male intruders for the replacement control task were adult (9–36 weeks), sexually experienced (proven or retired breeders) Swiss Webster (SW) males (Jackson Laboratory) housed at New York University Langone Medical Center (NYULMC). Mice were housed singly ($N = 18$ mice) or paired with females ($N = 58$ mice). The submissive males used in the SIA task and resident-intruder test and the castrated males used for the optogenetic activation experiments were adult (10–50 weeks), group-housed, and sexually inexperienced Balb/c males (Charles River). Mice were maintained on a reversed 12-h light/dark cycle (dark cycle starts at noon) and given food and water *ad libitum,* except during training and testing for the water control task, where they were only given access to water during the 40 min daily test session. All procedures were approved by the IACUC of NYULMC in compliance with the NIH guidelines for the care and use of laboratory animals.

Task design and training. The nosepoke apparatus for the self-initiated aggression (SIA) task consisted of two controllable infrared detector backlit nosepoke ports (Med Associates) attached 4.8 cm apart onto a transparent plastic panel. Prior to each training session, all items—including cage top, food, nesting material, and other mice (including female partners or pups, if any)—were removed from the cage and the noseport panel was inserted at one end of the cage. During the training, animals would receive access to the submissive male if they nose-poked into the right-hand port (relative to the animal when it faced the port) and continuously broke the infrared beam for a minimum of 100 ms. Once triggered, the beam could not be triggered until 5 s later to prevent multiple quick triggers during the wait period from being over-counted. After triggering the infrared beam, a submissive male would be manually placed in the cage from above after a wait of 3–7 s. During the reinforcement 'interaction' epoch, resident males received access to the submissive male for a variable interval of 5–10 s. Submissive male animals used for reinforcement were selected randomly from a group of five animals on each trial. If mice nosepoked the 'null' port, they received no access to the social reinforcement. Animals were provided with no additional learning incentives other than access to the submissive male at any time during training or testing. Mice used for the non-submissive replacement control task were equivalently sized, singly housed adult SW males with no defeat experience.

Mice were trained for 6–10 successive sessions of 35–40 min d^{-1} and animals were considered 'learned' if they reached poke rates of at least 0.2 pokes per min (one poke every 5 min) and reached performance levels of greater than 60% preference to the social-port on at least two successive days. Animals were trained at the same time each day. Two animals that exhibited extreme levels of aversion to the submissive male during the first few days of training were not trained for the full 10 days and were considered as not learned. We examined rates of spontaneous nosepoking in naïve animals who were never reinforced with the submissive male (or any other reward), and found that they were extremely low (first day poke rate (Mean ± STD) = 0.042 ± 0.02 pokes per min; second day poke rate = 0.075 ± 0.06 pokes per min, $N = 6$ mice), such that we found little evidence that animals will perform this task if unreinforced.

Animals trained on the water poking control task were water deprived for 12 h before initiating training. The same nosepoke apparatus was used, but with the addition of a water spout placed between the two nosepoke ports at snout level. Poking the right-hand port caused a droplet of water (~50 µL) to be released through a TTL-controlled solenoid following a 1-s delay. Animals were trained on successive training sessions of approximately 40 min/day and received a volume of 2–3 ml daily. Animals that reached a poke rate of 0.2 pokes per min and directed their pokes to the water port for 60% of trials were considered fully trained. Training on this task was often rapid and all animals ($N = 10$ mice) satisfied the learning criteria within 4 training days. For the reversal test, the reinforcement contingency was switched to the null port (100%) for four consecutive days, and then switched back to the social port until animals showed reversal behavior.

For the resident-intruder test, a submissive Balb/c male was placed into the home cage of the test SW male mouse for 10 min (pre-training aggression screening; **Fig. 1a**) or for 5 min (DREADDi inactivation resident-intruder experiments; **Fig. 5c,d**).

For the breakpoint test (**Supplementary Fig. 9**), animals already fully trained on the SIA task were trained for eight consecutive days using a progressive ratio schedule with a step size of 2 (PR2). Each session started with two fixed-ratio 1 (FR1) trials which had no time restriction and each successive reinforcement required an additional 2 pokes. If animals did not poke the social port within a minimum of 300 s of the previous poke, the breakpoint was considered to be reached.

Extracellular recording of freely moving mice. Methods for physiological recording in freely moving animals were described previously[21]. Custom-built 16-channel tungsten electrode bundles were attached to a moveable microdrive and implanted over the VMHvl (electrode coordinates: −1.7 mm anterior-posterior, 0.7 mm medial-lateral, 5.5 mm dorsal-ventral). After allowing 2 weeks for recovery, we connected the implanted electrode to a 16-channel headstage. Signals were streamed into a commercial acquisition system through a torqueless, feedback-controlled commutator (Tucker Davis Technology) and band-pass filtered between 100 and 5,000 Hz. Digital infrared videos of animal behavior from both side- and top-view cameras were simultaneously recorded at 640 × 480 pixel resolution at 25 frames per s (Streampix, Norpix). Video frame acquisition was triggered by a TTL pulse from the acquisition system to achieve synchronization between the video and the electrophysiological recording. Spikes were sorted manually using commercial software (OfflineSorter, Plexon) based on principal component analysis. Unit isolation was verified using autocorrelation histograms. To consider the recorded cell as a single unit, cells had to have a signal/noise ratio >2; spike shape had to be stable throughout the recording; and the percentage of spikes occurring with inter-spike intervals <3 ms (the typical refractory period for a neuron) in a continuous recording sequence had to be <0.1%. We checked for redundancies within days by examining the cross correlations of co-recorded neurons and checked for redundancies across days by comparing waveforms and temporal response profiles. After the first recording, the implanted electrode was slowly moved down in 40-µm increments. The placement of the electrode was examined histologically with the aid of DiI coated on the electrodes. Animals were excluded if electrodes were not confined to the VMHvl.

Fiber photometry. A rig for performing fiber photometry recordings was constructed following basic specifications previously described with a few modifications[26]. We injected a calcium indicator unilaterally into the VMHvl of task-naïve SW males. All viruses were purchased from UNC Vector Core or University of Iowa Gene Transfer Vector Core. During the surgery, a mixture of 120 nl of AAV2/1 CAG::Flex-GCaMP6s-WPRE-SV40 (Upenn, final titer:: 3.6×10^{11} PFU/ml) and AAV2/2 CMV::CRE (U. of Iowa, final titer: 1×10^{12} PFU/ml) was injected into the VMHvl unilaterally at 12 nl/min for each animal. Two animals were injected with 200 nl the same mixture into the MOB. (MOB coordinates: 3.7 mm anterior-posterior, 0.5 mm medial-lateral, 0.4 mm dorsal-ventral). GFP control animals were injected with 120 nl of AAV1 CAG::Flex-eGFP-WPRE-bGH (final titer:: 7×10^{12} PFU/ml) and AAV2/2 CMV::CRE (final titer: 1×10^{12} PFU/ml). A 400-µm optic fiber (Thorlabs, BFH48-400) housed in a ceramic ferrule (Thorlabs, CF440-10) was implanted 0.4 mm above the injection site. For MOB injected animals, fibers were placed directly on the surface of the bulb. After three weeks of viral incubation and before recording, a matching optic fiber was connected to the implanted fiber using a ferrule sleeve. A 400-Hz sinusoidal blue LED light (30 µW) (LED light: M470F1; LED driver: LEDD1B; both from Thorlabs) was bandpass filtered (passing band: 472 ± 15 nm, Semrock, FF02-472/30-25) and delivered to the brain to excite GCaMP6. The emission light then traveled through the same optic fiber, was bandpass filtered (passing band: 534 ± 25 nm, Semrock, FF01-535/50), detected by a femtowatt silicon photoreceiver (Newport, 2151) and recorded using a real-time processor (RZ5, TDT). The envelope of the 400-Hz signals that reflects the intensity of the GCaMP6 signals was extracted in real-time using a custom TDT program. The GCaMP6 signal was recorded during each training session (30–45 min d^{-1}) over a period of 10–21 d. Training sessions for fiber photometry consisted of a 3–5-min 'baseline' recording before the insertion of the nosepoke panel, followed by a 30–40-min SIA session. Baseline adjusted fluorescence signals for comparison across days were regressed using a 30s spline approximation. GFP control animals were tested for movement artifact by recording the fluorescence during a 15-min resident intruder test.

Stereotaxic injections for functional manipulation. All viruses were purchased from UNC Vector Core or University of Iowa Gene Transfer Vector Core. The viral titers mentioned below are the final titers in the injected solution.

For pharmacogenetic experiments, wild-type SW males were injected bilaterally into the VMHvl with a total of 280 nl/side of AAV2/2 Syn::DIO-DREADDi-mCherry (6×10^{12} PFU/ml) and AAV2/2 CMV::CRE (1×10^{12} PFU/ml) (VMHvl coordinates: −1.7 mm anterior-posterior, 0.7 mm medial-lateral, 5.75 mm dorsal-ventral) at 10 nl/min using a nanoinjector (World Precision Instruments), followed by an additional 5 min before retraction.

For optogenetic manipulation, wild-type SW males were injected bilaterally as above with a total volume of 120–200 nl/side of AAV2/2 EF1α::DIO-hChR2(H134R)-EYFP (2×10^{12} PFU/ml) and AAV2/2 CMV::CRE (1×10^{12} PFU/ml) into the VMHvl. To deliver light to the VMHvl, a double cannula (26G, 1.5 mm center-to-center distance, Plastics One) was implanted 0.8 mm above the injection sites and secured to the skull with dental cement (Metabond, Parkell).

EMG implantation and recording. We implanted animals with chronic EMG electrodes in the right masseter superficial muscles of the jaw (an important muscle for jaw closure). Electrodes were constructed using a pair of 0.001 inch flexible multi-strand stainless steel wires (A-M Systems, No. 793200) with the insulation removed from a 0.5-mm segment of each wire such that pairs of electrodes recorded signals from separate but nearby areas of the same muscle. Electrode wires were threaded through the muscle during a surgical procedure and anchored with a knot on the outside of the muscle. EMG wires were then threaded under the skin to the base of the skull where they were attached to ground electrodes. EMG wire output was relayed through a preamplifier and commutator to the digitizer with a sampling rate of 3,000 Hz (Tucker Davis Technology). Signals were processed by taking the difference from the pair of electrodes, and this differential signal was low pass filtered at 300 Hz. High-magnitude EMG events ("putative bites") were determined by detecting the number of times the EMG signal crossed a set threshold. The threshold was determined using the half maximum of either positive or negative polarity for each session of recording. For inactivation experiments, given that the animals did not always attack during CNO days, the threshold for EMG signal was determined based on recordings made during the interleaved saline-control days (**Fig. 5c,d**). For stimulation experiments, where comparisons were made between stimulation and sham trials within the same session, the threshold was set using the half-max of the whole session (**Fig. 6f,g**).

Pharmacogenetic inactivation. Following 2–3 weeks after injection of DREADDi virus (see above), animals were tested across successive days in the resident-intruder test, the SIA procedure, or the water poking control task (**Fig. 5b**). Tests were initiated 30 min after an i.p. injection of either 100 μL CNO (Sigma-Aldrich, Product No. 0832. Final concentration: 1 mg per kg of body weight diluted in saline) or 100 μl of saline. All animals were also tested on a rotarod task (5 min, rotation speed accelerating from 2.5–25 rpm) following each test session.

Optogenetic stimulation. Optogenetic testing was performed 2–3 weeks following viral injection and after a brief retraining (2–3 d) on the SIA task to restore the task performance to pre-surgery levels. To deliver light to the injection site, a single 230-μm multimode optic fiber (Thorlabs) was inserted into one side of the cannula and a dummy wire was inserted for stability into the other side. Fibers were secured with a matching cap (Plastics One). The other end of the optic fiber was connected to a 473-nm laser (Shanghai Dream Lasers) controlled by computer-programmed TTL pulses.

For optogenetic activation, animals were screened for 'functional' injection sites using a resident-intruder test to determine whether stimulation of each injection site was sufficient to evoke attack of a castrated Balb/c male. High frequency (10–20 Hz, 10-ms pulses, 0.5–1.5 mW) stimulation was delivered through the optic fiber for 20–30 s, with a minimum duration of 30 s between stimulation trials. Stimulated animals received 5–10 stimulation trials during each test session for each injection site (~15 min). Consistent with our previous report, light activation of functionally defined sites caused animal to orient toward, approach, investigate, and eventually attack the intruder[21].

During the SIA paradigm, animals were stimulated using lower frequency light (5–10 Hz, 10-ms pulses, 0.5–1.5 mW) during the interpoke interval. Real stimulation and sham stimulation (0 mW) were interleaved during the SIA task and stimulation was turned off automatically at the initiation of each nosepoke and manually restarted upon the removal of the submissive male. If animals did not poke within 10 min, the trial type was switched (that is, stimulation

was turned on or off) such that the maximum sham/real stimulation time for a single trial was 10 min. Functional injection sites were tested across three successive days in the SIA procedure to assess repeatability, while non-functional sites were tested for either once or twice.

Animals with functional injection sites were also tested using an RTPP test. Animals were placed into a two-chamber test arena (16.5×27 cm) where the chambers differed in both their floor material and lighting. Animals were permitted to freely roam the test arena during a 5-min pre-test. During the subsequent 10 min, one side of the chamber was paired with the same low frequency stimulation used during the SIA procedure. Stimulation pairing ceased for a 5-min post-test period. The time spent in each location during each of those epochs (pre, during, post) was then quantified using custom tracking software and normalized by the total time.

Histology and imaging. Animals were deeply anaesthetized using 0.5 ml of a ketamine-xylazine cocktail (10 mg/ml ketamine and 5 mg/ml xylazine) and transcardially perfused with phosphate buffered saline (PBS) followed by cold 4% paraformaldehyde in PBS. Brains were immersed overnight in a 20% sucrose solution, embedded with cutting medium (Tissue-Tek) and sectioned using a cryostat (Leica). Standard immunohistochemistry procedures were followed to stain 30-μm coronal brain sections for all mice. DAPI (1:20,000, Life Technologies, catalog number D21490, widely validated) was used to assess electrode track for physiology and fiber track for photometry. We acquired 2.5× or 5× fluorescent images to determine cannula or electrode placements. We used 10× fluorescent images to count GCaMP6 and DREADDi-mCherry cells. Cell counting was done manually using ImageJ on 30-μm sections separated by 60 μm. For GCamP6-labeled neurons, neurons in an area determined by the numerical aperture of the fiber (NA = 0.48) were counted on sections with a visible fiber track. Percent of labeled neurons in the VMH was calculated as (GCaMP6 labeled neurons in VMH/Total number of GCaMP6 neurons in light cone) × 100. Percent of total neurons labeled was calculated as (GCaMP6 labeled cells / total neurons in the VMH) × 100.

Behavioral analyses. Custom software written in Matlab (MathWorks) was used to facilitate frame-by-frame manual annotation of mouse behavior using simultaneously acquired side- and top-view videos (https://github.com/pdollar/toolbox). Investigation was defined as nose-to-face, nose-to-trunk, or nose-to-urogenital contact. Attacks were defined by a suite of actions initiated by the resident toward the male, which included lunges, bites, tumbling, and episodes of fast locomotion between such behaviors. During stimulation, behaviors such as freezing and cornering were also identified visually. Top-view videos were used to extract movement velocity and animal position during the SIA and RTPP tests on a frame-by-frame basis, and epochs of social interaction were excluded from these analyses. An LED light that was synchronized with optogenetic stimulation was placed in view of the camera for *post hoc* confirmation of video synchronization. Poke rates and poke timing during the SIA and water control task were assessed using the infrared detector and did not rely on manual video analysis.

Statistical analyses. Parametric tests, including Student's *t*-test, paired *t* test, and two-sampled *t* test were used if distributions passed Kolmogorov–Smirnov tests for normality. For within-neuron tests of firing rate significance, a nonparametric Wilcoxon signed rank test was used since spike rates were often low and not normally distributed. Repeated tests of significance were corrected with a false discovery rate (FDR) correction. For all statistical tests, significance was measured against an alpha value of 0.05 unless otherwise stated. All error bars show s.e.m. No statistical methods were used to predetermine sample sizes, but our sample sizes are similar to those reported in previous publications[20,23,26]. Data here was collected and processed in blocks by methodological subtype and animals were assigned to various experimental groups in blocks after task training. Data collection and analysis were not performed blind to the conditions of the experiments.

Statistical analyses used in each figure are listed below.

Figure 1. (**f**) Unpaired two sample *t*-test. (**g**) Task learning is defined as number of days to reach the learning criteria. (**h**) Paired *t*-test between the last days of each reversal, *t*-tests on individual days compared to a null distribution of 50%. (**j**) Paired *t*-test.

Figure 2. (**a**–**f**) PETHs were plotted using 1s bins aligned to the poke initiation for each trial with no smoothing. (**g**) Activity matrix was constructed by computing Z-score transformed PETH for each neuron aligned to the nosepoke and then sorted based on the peak time (169 neurons, −8 s before poke to 8 s after poke using 1-s bins). (**h**) Principal components were extracted using single variable decomposition of activity matrix shown in (**g**). (**i**) Within neurons significance assessed using repeated Wilcoxon signed rank test with FDR correction on trial-to-trial rate in interaction bin (0–3 s after introduction), wait bin (1–3 s after poke), and poke bin (−1 s to 1 s around poke) to trial-to-trial activity during the interpoke interval (−15 s to −1 s before poke). Neurons for a particular time bin were classified as "increased" if mean activity was greater than mean activity during the IPI and $P < 0.05$. Neurons were classified as "decreased" if mean activity was less than mean activity during the IPI and $P < 0.05$. All neurons with $P \geq 0.05$ were classified as "no-change".

Figure 3. GCaMP6 activity traces in (**d**,**e**) show raw signal. Baseline adjusted GCaMP6 signals (**f**–**i**) for comparing across days were computed by regressing the baseline using a spline approximation using a moving 30-s window. For display purposes in (**f**), the y-intercept for each day was subtracted. Slopes (**g**,**i**) were computed by linearly regressing the raw GCaMP6 activity −2 s to 0.5 s around nosepoke. Fits were performed on (**g**) using nonlinear fit with the equation: $F(x) = A(1) + A(2) / (1 + exp(−(x − A(3)) / A(4)))$ where x is training day, which minimized the RMSE more than either first or second order polynomial fits. (**h**) Mean normalized response across trials for 5 animals for early training (red, first 4 days, $n = 47$ trials; blue last 4 days, $n = 424$ trials). (**i**) Paired t-test for comparison of early and late slope population means and student's t-test for individual animals slope distributions for early and late train epochs.

Figure 4. (**c**,**f**) Plots show baseline adjusted (as in **Fig. 3f**). Slopes (**e**) were computed as above and fit for each days (extinction days 0–2) using least-squares regression. (**e**,**g**) Paired t-test of extinction day 0 to extinction day 1 and extinction day 2.

Figure 5. (**c**) EMG threshold was set using the half-max value during the saline day. (**d**) Putative bite number was computed by the number of threshold crossings during saline and CNO test days and compared with paired t-tests. (**f**,**g**) Single factor, repeated measures ANOVA.

Figure 6. (**e**,**g**) Paired t-tests. (**f**,**g**) Putative bite rates were computed for each interaction (number of threshold crossings / interaction time) and mean rates were computed for each test session separated by interactions preceded by sham stimulation or real stimulation. Sham and stim threshold crossing rates were averaged across multiple days of testing.

Supplementary Figure 1. (**a**,**b**) Paired t-test between poking rate of social-port or water-port and that of null-port for each training day. (**c**,**d**) Paired t-test between behavioral test day and pre-test control day (gray bar).

Supplementary Figure 2. (**c**) Activity matrix of neurons sorted by their time point of maximal activation and clustered into four distinct groups (Ward's method). Cluster identities were preserved using cross validation, were affirmed using a second clustering algorithm (k-means), and are consistent with principal components analysis (**Fig. 2h**).

Supplementary Figure 3. (**d**,**e**) Slope analysis as in **Figure 3**.

Supplementary Figure 4. (**e**) Power/Frequency curve computed using fast Fourier transform of raw activity during example quiet epoch shown in (**d**).

Supplementary Figure 6. (**b**,**c**,**e**,**f**) Single factor, repeated measures ANOVA.

Supplementary Figure 8. (**c**) Cumulative distribution of attack initiation times relative to the onset of stimulation. Each point represents the probability of an attack having been initiated at that time point for each trial where 0 represents no attack and flips to 1 if an attack has been initiated. Plot is averaged across all trials for all functional sites for animals in shown **Figure 6**. Bar plot represents the averaged percent of stimulation trials showing attack across all functional sites. (**f**) Paired t-test. (**g**) Heat map computed using tracking results normalized by total time spent in the RTPP test. (h) Single factor, repeated measures ANOVA.

Supplementary Figure 9. (**f**) Paired t-test

A **Supplementary Methods Checklist** is available.